A new bi-imaging NDT system for simultaneous recovery of attenuation and electronic density maps

Cécilia Tarpau[1,2,3*], Javier Cebeiro[4] and Mai K. Nguyen[1]

[1] Equipes de Traitement de l'Information et Systèmes, University of Cergy Pontoise, ENSEA, Cergy Pontoise, France
[2] Laboratoire de Physique Théorique et Modélisation, University of Cergy Pontoise, Cergy Pontoise, France
[3] Laboratoire de Mathématiques de Versailles, University of Versailles Saint Quentin, Versailles, France
[4]Centro de Matemática Aplicada, Universidad Nacional de San Martín, Buenos Aires, Argentina
*corresponding author, E-mail: cecilia.tarpau@ensea.fr

Abstract

Computed Tomography is a widely used imaging technique for non-destructive testing and evaluation in industry. Tomographic modalities exploit only primary radiation, which is non-deviated but attenuated radiation going through matter. However, in the energy range of X and gamma rays used in non destructive testing, Compton effect is an important physical phenomenon which should be taken into account. Compton Scattering Tomography is precisely the imaging technique, which not only accounts for the Compton effect but also uses it to image material electronic density. This paper proposes the concept of a Compton scanner, which is formed by a source and several detectors placed on a circular ring. When the detectors are set to register the energy of primary photons, the system works as Fan-Beam computed tomography scanner. But if the detectors are set to register the energy of scattered photons, the system operates as Compton scattering tomography scanner. Such a device, that we called a bi-imaging system provides both the attenuation map and the electronic density of the scanned object. Both information from primary and scattered rays is then wisely exploited. The mathematical modelling of this system makes use of a Radon transform on circular arcs. Numerical simulations are carried out in order to illustrate the theoretical feasibility of the proposed system.

1. Introduction

Computed Tomography (CT) is one of the conventional non-invasive technology mostly used in industry [1]. The imaging process is based on radiation attenuation through the matter along linear paths and described by the Beer-Lambert law

$$I(E,L) = I_0(E)\exp\left(-\int_{(x,y)\in L}\mu(x,y,E)d\ell\right) \quad (1)$$

where $I_0(E)$ and $I(E,L)$ are respectively the intensity of emitted and transmitted photons at energy E on the considered line L and $\mu(x,y,E)$ is the attenuation coefficient of pixel (x,y) at photon energy E. Image reconstruction consists in the recovery of the attenuation map μ from data projections and is achieved by the analytical inversion of the classical Radon transform on straight lines, the mathematical tool which models this imaging process [2, 3].

However, in the middle energy range $0.1 \sim 5$ MeV and particularly for materials with a low atomic number, Compton scattering is the predominant phenomenon responsible of a decrease of radiation energy [4]. Moreover, considering an initial photon flux at energy E_0, Compton scattering is characterised by a deflection of photons from its initial path with an angle ω, related to the energy of the photon flux $E(\omega)$ after the scattering process :

$$E(\omega) = \frac{E_0}{1+\frac{E_0}{m\,c^2}\,(1-\cos(\omega))}, \quad (2)$$

with $m\,c^2$ the energy of the electron at rest.

CT modalities attempt to eliminate these scattered radiation especially by the use of collimators, and we estimate that only 1/10000 photon arrives at the detector due to their presence [5]. This is characterized by a lost of contrast at reconstruction. Previous studies showed that scattered radiation is a useful part of information and, consequently, can also be used for tomographic reconstruction. This statement notes the emergence of Compton Scattering Tomography modalities [5, 6].

1.1. Working principle and advantages of Compton scattering tomography

Figure 1 illustrates the working principle of Compton Scattering Tomography (CST). A source S emits primary rays, which are passing through an object. These primary rays are scattered at different scatter sites M_i of the object and a detector D collects the intensity of scattered photons according to their energy $E(\omega)$.

Simple geometric considerations show that, given the locations of the source S and the detector $D_k, k \in [|1,K|]$,

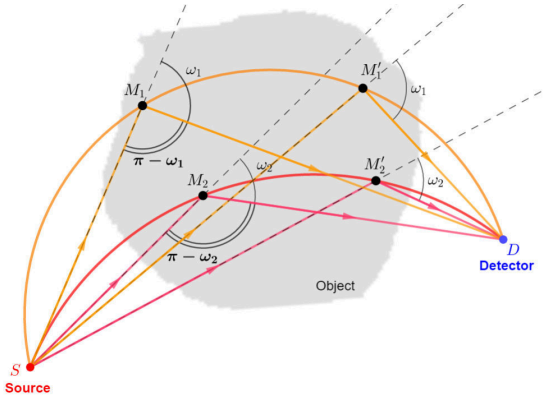

Figure 1: General scheme of CST modalities

scattering sites corresponding to the same deflection of angle ω are located on a circular arc passing through S and D and subtending the angle $(\pi - \omega)$. Consequently, image acquisition and reconstruction processes for CST modalities are respectively modelled by the forward and inverse Radon transforms on families of circular arcs, according to the geometry of the considered modality.

CST offers several advantages for non-destructive inspection :

- the possibility to have the source and the detector on the same side of the sample, particularly suitable for scanning large objects like walls, installed aircraft sections or large filled storage tanks [7],
- a higher contrast with the potentiality to have a better resolution and sensitivity,
- the possibility to have fixed systems [8, 9, 10] (without any mechanical rotation)

Potential advantages for CST modalities in aircraft non-destructive testing are the detection of corrosion and cracks in aluminium and more generally in composite aircraft panels or the detection of damage and disbonding in honeycomb structures [11].

Compton scattering offers also the possibility of backscatter imaging, the reader can refer to [12, 13, 14, 15, 16].

1.2. Review on previous proposed modalities

The first CST modality, proposed by Norton [8], is composed of a fixed source S and fixed detectors D placed along a line passing through the source (see Figure 2). This modality has been studied from a theoretical point of view, in order to provide exact inversions of the associated Radon transform (first by Norton in [8] and next by Rigaud in [17, 18]) and then under more realistic conditions for corrosion detection in [7]. One can also note the proposition of an *improved* version of this modality in [19].

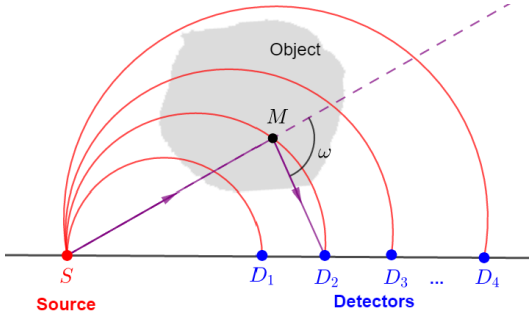

Figure 2: Norton's modality

The second modality [20] proposed by Nguyen and Truong, which uses a source and a detector diametrically opposed in rotation around the object has applications in biomedical imaging.

1.3. A new modality of Compton scattering tomography

A new CST modality (see Figure 3), named Circular Compton Scattering Tomography [9, 10, 21, 22] has been recently proposed. This modality is made of a source and detectors placed on a ring passing through the source.

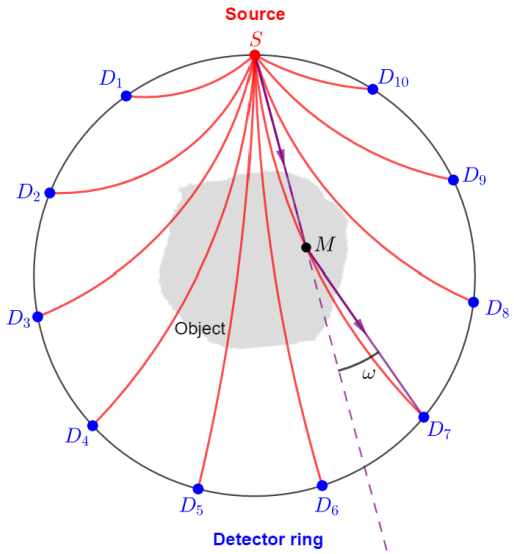

Figure 3: Circular Compton Scattering Tomography

Such a modality has the following advantages :

- CCST is able to recover all information of scattered radiation needed for reconstruction using non-moving source and detectors.
- The CCST setup is more compact than those from modalities with detectors placed on a line.

- CCST is suitable for small objects scanning and also offers the possibility of one-side scanning [21].

Image formation is modelled by the new Radon transform on circular arcs, with a fixed end, the point Source. The other end-point is located on a circle (the detector ring). For the case where attenuation is neglected, an exact reconstruction formula has been provided in [21].

1.4. Purpose of the paper

The purpose of this paper is two-fold : first, we explore an additional advantage of the new CCST modality. In fact, CCST has the same geometry as the well-known Fan-Beam Computed Tomography. The objective is to propose a new bi-imaging system combining Fan-Beam CT (FBCT) and CCST. Thus, this imaging system offers the access to two types of information: the attenuation map with the FBCT mode and the electronic density exploiting scattered radiation with CCST. A combination of ordinary transmission techniques and CST has been originally envisaged by [23] for a system composed of one source and one detector.

Second, we propose a new algorithm which exploits the attenuation map obtained by the FBCT mode to tackle the attenuation problem for the CCST mode. This constitutes an advance over previous works about CCST modalities where attenuation is absent in the acquisition modelling for the sake of invertibility of the corresponding generalized Radon transform. This algorithm is based on the exact reconstruction formula of the corresponding non-attenuated Radon transform on circular arcs where we apply iterative correction steps thank to the *a priori* knowledge of the attenuation map via FBCT. This algorithm can be seen as the adaptation of the Generalized Chang Correction (GCC) algorithm [24, 25] for a CST modality.

Section 2 introduces the bi-imaging system with its two modes. Section 3 describes the reconstruction algorithm of the attenuated Radon transform on circular arcs, modelling the imaging process for the CCST mode. Numerical simulation results are shown in Section 4 for a multi-layer composite material. Perspectives for future work are proposed in Section 5.

2. A bi-imaging system combining Fan-Beam CT and CCST

In the rest of the paper, f denotes either the original attenuation map in FBCT mode or the original electronic density when the system work as CCST.

From the observation that both CCST and Fan-beam computed tomography have a similar geometry, we propose here the design of a unique system (see Figure 4), sharing a mono-energetic source and multi-energy range detectors, to recover both attenuation map and electron density of the object.

2.1. General setup of the bi-imaging system

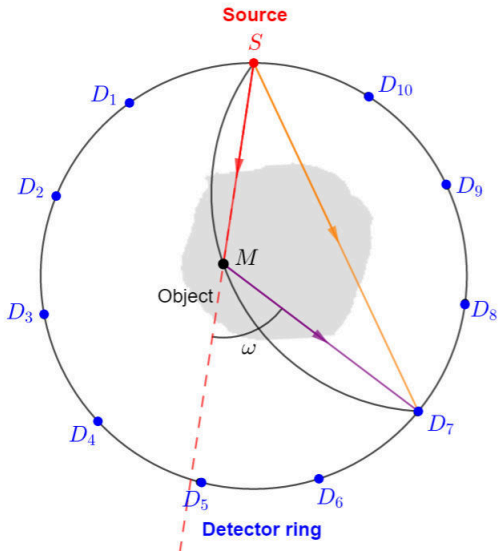

Figure 4: Bi-imaging system combining Fan-Beam CT and CCST - In orange : transmitted photon path at energy E_0 recovered in the FBCT mode - In red : emitted photon path scattered at point M - In purple : scattered photon path at energy E_ω in CCST mode

The mode of the system is chosen from the energy range recovered by the detector. If the detectors are set to register transmitted photon at energy E_0 (that is the energy of emitted photons), the system works as Fan-Beam CT. This setup needs the mechanical rotation of the system in order to recover the complete data set of projections. Otherwise, if the detectors recover radiation from the energy range $]E_0, E(\pi)[$ (according to the Compton formula), then the system records scattered radiation and works in the CST mode.

2.2. Data measurement with the Fan-beam CT mode

In the FBCT mode (Figure 5), data are required along lines originating from the point source and spreading towards the detectors. As for the parallel beam, the system needs to rotate to have all projections.

From data projections $\mathcal{R}_{fan}f$ at energy E_0, one can reconstruct the attenuation map $\mu(E_0)$ (see Eq.(1)). The particular case of Fan-beam CT has been widely studied in the literature and will be no longer explained in this paper. The reader can refer for example to [26]. In the rest of the paper, we note μ_{fan} the obtained attenuation map with FBCT.

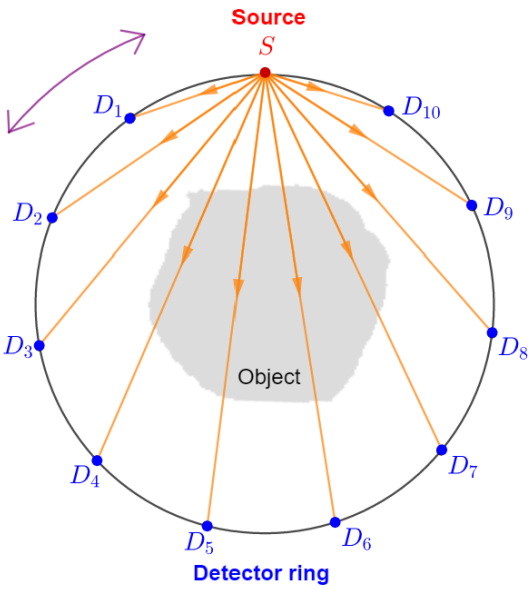

Figure 5: Fan-beam CT mode

2.3. Data measurement from the CCST mode

2.3.1. Setup of the model (see Figure 6)

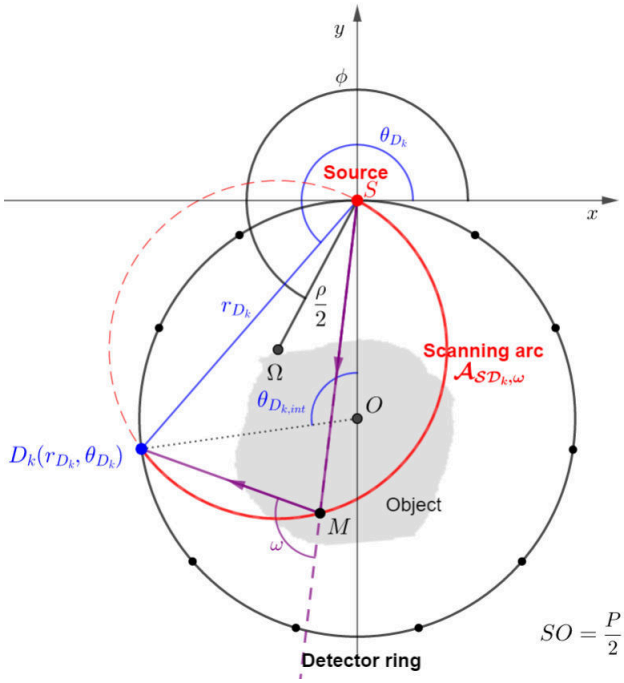

Figure 6: Setup of the CCST mode

The source S is placed at the origin of the system and the K detectors D_k (with $k \in \{1, 2, ..., K\}$) are placed on the ring of polar equation :

$$r = P \cdot \cos\left(\theta + \frac{\pi}{2}\right), \text{ where } \theta \in [\pi, 2\pi[. \tag{3}$$

The localization of each detector on this ring is identified by the angle $\theta_{D_{k,int}}$

$$\theta_{D_{k,int}} = 2\pi \frac{k}{K+1}, \tag{4}$$

which is itself related to polar angular coordinate θ_{D_k} of the considered detector:

$$\theta_{D_k} = \pi + \frac{\theta_{D_{k,int}}}{2}. \tag{5}$$

Using previous equations (4) and (5), the polar coordinates (r_{D_k}, α_{D_k}) of each detector D_k are :

$$D_k(r_{D_k}, \theta_{D_k}) \text{ with } \begin{cases} r_{D_k} &= P \cos\left(\theta_{D_k} + \frac{\pi}{2}\right) \\ \theta_{D_k} &= \pi\left(1 + \frac{k}{K+1}\right). \end{cases} \tag{6}$$

2.3.2. Parametrization of the scanning arcs

Data acquisition is performed on scanning arcs denoted in the rest of the paper $\mathcal{A}(SD_k, \omega)$ of equation

$$\mathcal{A}(SD_k, \omega\,;\ \rho, \phi) : r = \rho \cdot \cos(\theta - \phi), \tag{7}$$

where

$$\begin{cases} \rho(D_k, \omega) &= \frac{r_{D_k}}{\sin(\omega)} \\ \phi(D_k, \omega) &= \theta_{D_k} + \omega - \frac{\pi}{2}, \end{cases} \tag{8}$$

$$\theta \in \begin{cases} [\theta_{D_k}, \theta_{D_k} + \omega] & \text{if } \phi \in \left[0, \frac{3\pi}{2}\right] \\ [\theta_{D_k} + \omega, \theta_{D_k} + \pi] & \text{if } \phi \in \left[\frac{3\pi}{2}, 2\pi\right]. \end{cases} \tag{9}$$

2.3.3. Associated Radon transform on circular arcs (CirArcRT)

Data measurement leads to the Radon transform on circular arcs (CirArcRT) whose equation is

$$\mathcal{R}_{\mathcal{A}} f(\rho, \phi) = \int_{\mathcal{A}(SD_k, \omega\,;\ \rho, \phi)} f(r, \theta)\, ds, \tag{10}$$

where ds is the integration element of the circular arc $\mathcal{A}(SD_k, \omega)$.

Image reconstruction requires the inversion of the CirArcRT, that is $\mathcal{R}_{\mathcal{A}}^{-1} f$. This inversion is achieved in [21]. However, this algorithm does not take into account attenuation in the matter. This problem is tackled in the next paragraphs by the introduction of a new correction algorithm for image reconstruction from attenuated scattered radiation.

2.3.4. Taking into account attenuation for the modelling of the imaging process

As mentioned previously, an object is reconstructed from a data set of projections along circular arcs in the CCST mode.

However, these projections are affected by attenuation in different ways on two paths: attenuation a_1 concerning the emitted photon at initial energy E_0 from the source S to the scattering site M and attenuation a_2 relative to scattered photon at energy $E(\omega)$ from M to the considered detector D_k (ω being the scattering angle):

$$a_1(E_0, SM) = \exp\left(-\int_{J\in SM} \mu(E_0, J)\, dl(J)\right), \tag{11}$$

$$a_2(E(\omega), MD_k) = \exp\left(-\int_{J\in MD_k} \mu(E(\omega), J)\, dl(J)\right). \tag{12}$$

Consequently, taking into account attenuation for the modelling of data measurement leads to an attenuated Radon transform on circular arcs (CirArcRT$_{\text{att}}$):

$$\mathcal{R}^{att}_{\mathcal{A}} f(SD_k, \omega) = K(\omega)\cdot \int_{M\in\mathcal{A}(SD_k,\omega)} a_1(E_0, SM)\, f(M)\, a_2(E(\omega), MD_k)\, dl(M), \tag{13}$$

where $K(\omega)$ is the kinematic factor of the Compton effect [27].

To the authors knowledge, the exact inversion formula of Eq.(13) has not been found for any of the CST modalities. To overpass this problem, a previous iterative algorithm based on the exact inversion formula for the non-attenuated Radon transform corresponding to Nguyen's modality has been proposed in [27, 28]. This algorithm supposes the knowledge of the different kinds of matter of the object, and approximates the attenuation map of the object to correct the reconstruction of electronic density. This attenuation-correction allows the improvement of the quality of reconstruction, but is however slow (10 iterations are needed to reduce the initial error by half, according to [28]).

In this article, we propose to take advantage of the *a priori* knowledge of the attenuation map thank to the Fan-Beam CT mode to correct data obtained with scattered radiation. This new algorithm is presented in the next section.

3. A new correction algorithm for image reconstruction from attenuated scattered projections

3.1. General assumption

For the proposed algorithm, it was assumed that attenuation is independent of the energy of the considered ray. In other words, the Radon transform solved by our algorithm is

$$\mathcal{R}^{att}_{\mathcal{A}} f(SD_k, \omega) = K(\omega)\cdot \int_{M\in\mathcal{A}(SD_k,\omega)} a_1(SM)\, f(M)\, a_2(MD_k)\, dl(M), \tag{14}$$

where

$$a_1(SM) = \exp\left(-\int_{J\in SM} \mu(J)\, dl(J)\right) \tag{15}$$

$$a_2(MD_k) = \exp\left(-\int_{J\in MD_k} \mu(J)\, dl(J)\right). \tag{16}$$

Here, coefficient μ is independent of the energy and, consequently, factors a_1 and a_2 are also independent. This condition is reasonable if scanning acquisition is performed in the lower part of the energy range where Compton effect is predominant, and for low-Z materials, like carbon and aluminium. A discussion about a possible improvement which allows avoiding such assumption is proposed in Section 5.

3.2. Correction method

The proposed algorithm consists in the *a posteriori* correction of the reconstruction obtained through the exact inversion formula of the CirArcRT. To this end, we use the approximation of the attenuation map obtained from the Fan-Beam CT scanning. The initial reconstruction is denoted in the rest of the paper f_0. Each pixel of the image $f_0(i,j)$ is weighted then by a correction coefficient $c(i,j)$ that takes into account the average effect of attenuation for this point. To do this, we compute first an intermediate variable c_d for each pixel (i,j), which sums the attenuation coefficients along every path where the corresponding point is a scattering site according to the equation

$$c_d(i,j) = \sum_{M(i,j)\in\mathcal{A}(SD_k,\omega)} \exp\left(-\int_{J\in SM} \mu_{fan}(J) dl(J)\right) \times \exp\left(-\int_{J\in MD_k} \mu_{fan}(J) dl(J)\right) \tag{17}$$

and, finally, we obtain $c(i,j)$ weighting $c_d(i,j)$ in (18) by the number of times $N_p(i,j)$ where the pixel is a scattering site (and, by this way, obtain a mean value)

$$c(i,j) = \left(\frac{1}{N_p(i,j)}\cdot c_d(i,j)\right)^{-1}, \tag{18}$$

The product $c \cdot f_0$ is the first order correction and allows to obtain the first order corrected image denoted f_1. The second order step is common with the GCC algorithm, and consists in acquiring projections from the corrected image f_1. We compute the error on projection by subtracting data acquisition from the corrected image and data acquisition from the original object. The error made on reconstruction is then obtained by applying the inverse of the CirArcRT ($\mathcal{R}_{\mathcal{A}}^{-1} f$) to the error projection and weighting by the correction matrix c using Eq.(17). The second order corrected image f_2 is finally obtained with the addition of the error object to f_1.

The second order step can be repeated as much as is necessary to finally obtain f_n at the n-th order step. The reconstruction algorithm is summed up in Figure 7.

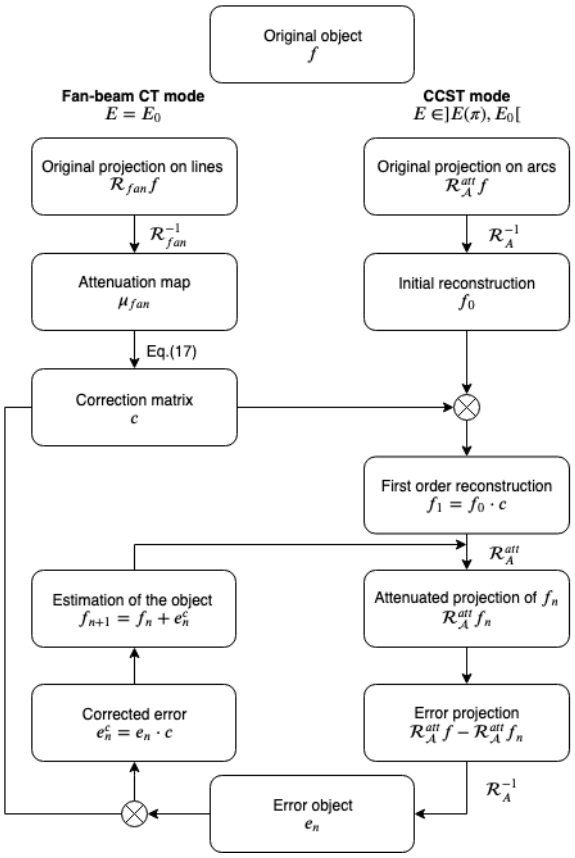

Figure 7: Reconstruction of the electronic density of the object f

4. Simulation results

4.1. Chosen phantom

The phantom chosen for simulation is a multi-layer composite material with three different matters. The size of the object is $N \times N = 128 \times 128$.

Attenuation coefficients and electronic density used for this simulation are given for the three materials in Table 1 and shown in Figure 8 and Figure 9. Both electronic densities and attenuation coefficients of the three materials are chosen arbitrarily. In fact, this simulation with this phantom has only the objective to validate the proposed attenuation correction algorithms. Other simulations with more realistic objects will be done in future works.

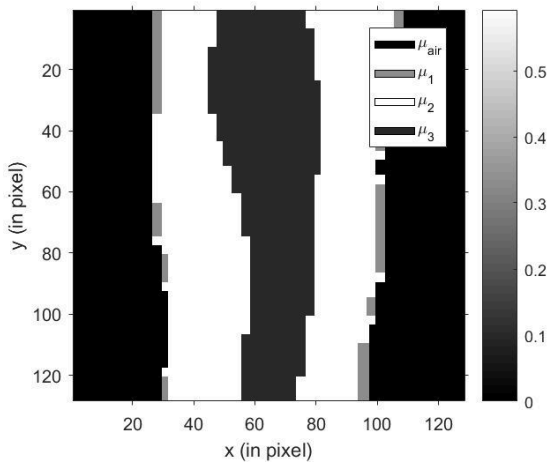

Figure 8: Attenuation map of the multi-layer phantom

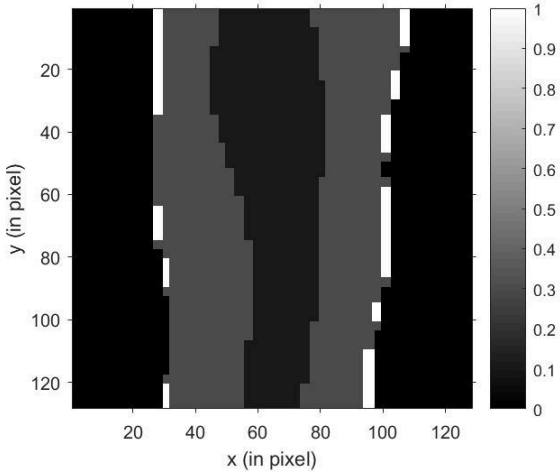

Figure 9: Electronic density of the multi-layer phantom

Table 1: Attenuation coefficients and electronic density (in cm^{-1}) of the three materials

material	attenuation coefficient μ_i (in cm^{-1})	electronic density $n_{e,i}$ (in cm^{-1})
air	$\mu_{air} = 0$	$n_{e,air} = 0$
material 1	$\mu_1 = 0.33$	$n_{e,1} = 1$
material 2	$\mu_2 = 0.59$	$n_{e,2} = 0.3$
material 3	$\mu_3 = 0.28$	$n_{e,3} = 0.1$

The visual evaluation of the quality of reconstruction will be completed by the use of the Normalized Mean Squared Error (NMSE) metric, defined as

$$\text{NMSE} = \frac{\sum_{(i,j)\in[|1,N|]^2} (I_o(i,j) - I_r(i,j))^2}{\max_{(i,j)\in[|1,N|]^2} I_o(i,j)^2} \cdot \frac{1}{N^2} \quad (19)$$

where I_o and I_r are respectively the original and the reconstructed images.

4.2. Parameter choices for the bi-imaging system

The phantom is placed inside a detector ring of radius equal to the side of the system, that is 128 length unities. On the ring, detectors are uniformly distributed, one detector each two length unities. This represents a amount of $N_D = 804$ detector on the ring.

For the fan-beam CT mode, the chosen rotation increment is 1 degree.

For the CCST mode, the number of scanning arcs per detector is $N_\omega = 500$. In fact, we know that $N_D \times N_\omega$ should satisfy the well-known condition

$$N_D \times N_\omega \geq N \times N, \quad (20)$$

given in [29] for the ideal case of uniform sampling without missing data and no noise. Moreover, this condition has to be over-estimated in our case, because the acquisition on circular arc does not satisfy the condition of uniform sampling.

4.3. Obtained attenuation map with FBCT mode

Data acquisition and reconstruction for Fan-Beam CT mode is performed using preinstalled functions provided by Matlab. The functions are adjusted according to the parameter choices given in the previous section. Figure 10 shows the reconstructed attenuation map.

4.4. Data acquisition and obtained electron distribution with CCST mode

4.4.1. Data acquisition

Figure 11 shows the result of image acquisition in the CCST mode. For a larger discussion, about data acquisition with the CCST modality, one can refer to [9, 21, 22].

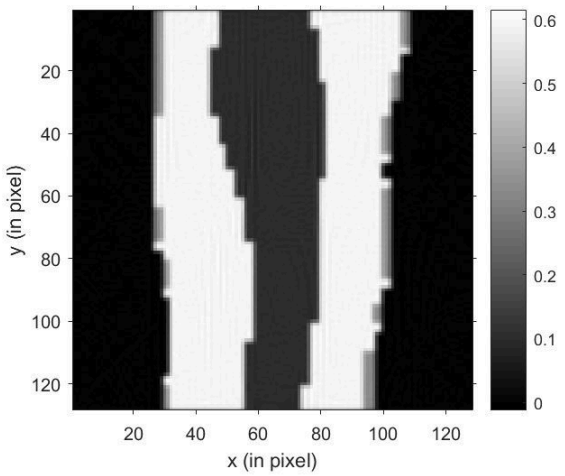

Figure 10: Reconstruction of the attenuation map μ_{fan} with Fan-Beam CT mode - NMSE = 0.0009

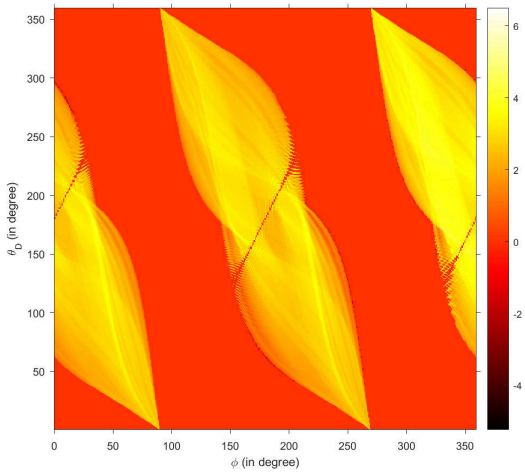

Figure 11: Data acquisition from the electronic density map $\mathcal{R}^{att}_{\mathcal{A}} f$ with CCST mode in a logarithmic scale

4.4.2. Results of image reconstruction

Figure 12a, 12b, 12c and 12d show the different steps of reconstruction obtained with the proposed iterative algorithm. Figure 12a shows the result of initial reconstruction, that is the first reconstruction obtained with the inverse non-attenuated Radon transform. This reconstruction gives a good result of the structure of the layer but we can observe that there is a non-homogeneity between the top and the bottom of the reconstruction. The reader can observe that this non-homogeneity is corrected by the first order step (see Figure 12b), although NMSE doesn't decrease during this step. The next steps (Figures 12c and 12d) allow having a better contrast between the different layers and reducing initial NMSE by half.

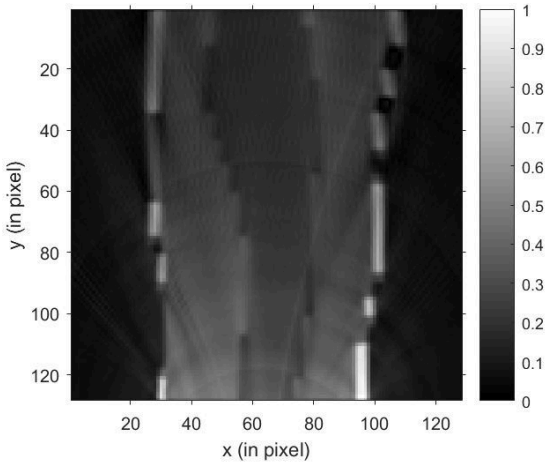

(a) Initial reconstruction f_0 - NMSE = 0.0168

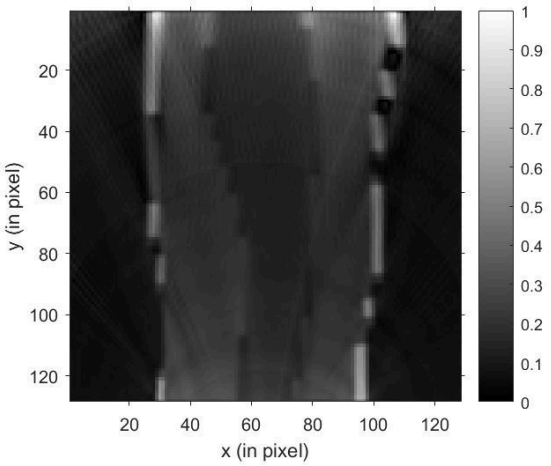

(b) First order reconstruction f_1 - NMSE = 0.0176

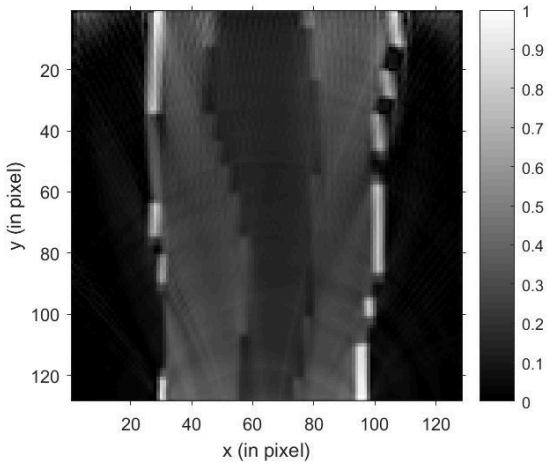

(c) Second order reconstruction f_2 - NMSE = 0.0092

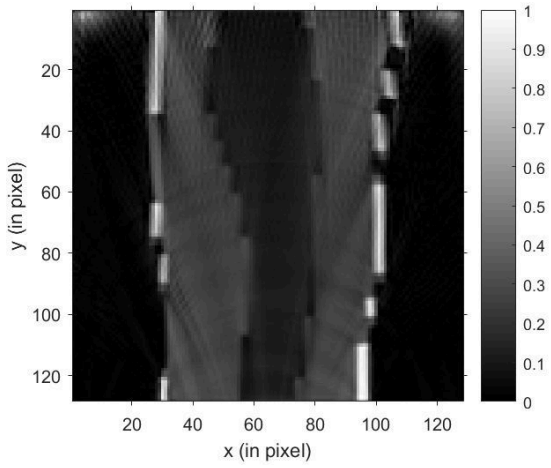

(d) Third order reconstruction f_3 - NMSE = 0.0083

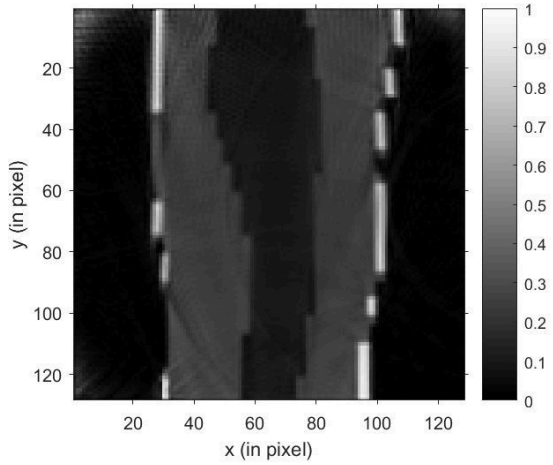

(e) Image reconstruction with two data acquisitions and three iterations - NMSE = 0.0066

Figure 12: Reconstruction of the electronic density map of the multi-layer phantom

4.5. Improvement of image quality of electronic with a second data acquisition

The quality of image reconstruction can be also improved combining reconstructions from two data acquisition of electronic density. In this study, we propose to combine the reconstructions from two data acquisitions corresponding to source positions shifted $\pi/2$ one from the other. This second acquisition of electronic density does not increase the complexity of our system : in fact, the system has to rotate for the Fan-Beam CT mode and the use of multi-energy range detectors for this system allows to recover intensity of scattered photons for each source position. Intensities of scattered photons have just to be recorded for another position of the source. The final reconstruction is then obtained by numerically combining the two results (see Figure 12e).

5. Discussions and perspectives of this work

This study gives the first simulation results for an iterative reconstruction method based on exact reconstruction formula of the CirArcRT. This result opens new perspectives which will be studied in future works:

- Study other attenuation correction algorithms to take into account attenuation such as [25] for the bimodality.
- Enlarge the proposed algorithm to take in account the dependence of attenuation relative to energy.
- Extend this study for the CCST with Monte Carlo simulations and real phantoms.

Acknowledgement

C. Tarpau research work is supported by grants from Région Ile-de-France (in Mathematics and Innovation) 2018-2021 and LabEx MME-DII (Modèles Mathématiques et Economiques de la Dynamique, de l'Incertitude et des Interactions) (No. ANR-11-LBX-0023-01).
J. Cebeiro is partially suported by SOARD-AFOSR (grant number FA9550-18-1-0523) and by a CONICET postdoctoral grant (Leg. 171800).
The authors would like to thank also the Institute for Advanced Studies (IAS) of the University of Cergy Pontoise in France for the financial support given to this research project.

References

[1] L. De Chiffre, S. Carmignato, J.-P. Kruth, R. Schmitt, and A. Weckenmann, "Industrial applications of computed tomography," *CIRP annals*, vol. 63, no. 2, pp. 655–677, 2014.

[2] J. Radon, "Über die Bestimmung von Funktionen durch ihre Integralwerte längs gewisser Mannigfaltigkeiten," *Akad. Wiss.*, vol. 69, pp. 262–277, 1917.

[3] A. M. Cormack, "Representation of a function by its line integrals, with some radiological applications," *Journal of Applied Physics*, vol. 34, no. 9, pp. 2722–2727, 1963, [doi:10.1063/1.1713127].

[4] F. M. Khan and J. P. Gibbons, *Khan's the physics of radiation therapy*. Lippincott Williams & Wilkins, 2014.

[5] T. Truong and M. K. Nguyen, "Recent developments on Compton scatter tomography: theory and numerical simulations," in *Numerical Simulation-From Theory to Industry*. IntechOpen, 2012, [doi:10.5772/2600].

[6] R. Xiao, S. Sato, C. Uyama, and T. Nakamura, "Fundamental study of Compton scattering tomography," Tech. Rep., 1994.

[7] B. L. Evans, J. Martin, L. Burggraf, and M. Roggemann, "Nondestructive inspection using Compton scatter tomography," *IEEE Transactions on Nuclear Science*, vol. 45, no. 3, pp. 950–956, 1998.

[8] S. J. Norton, "Compton scattering tomography," *Journal of applied physics*, vol. 76, no. 4, pp. 2007–2015, 1994, [doi:10.1063/1.357668].

[9] C. Tarpau and M. K. Nguyen, "A novel modality of Compton Scattering Tomography, Image formation and Reconstruction," in *Proceedings of the International Conference on Image Processing, Computer Vision, and Pattern Recognition (IPCV'19)*, Las Vegas, United States, Jul. 2018, pp. 60–65.

[10] J. Cebeiro, M. K. Nguyen, M. Morvidone, and C. Tarpau, "An interior Compton Scatter Tomography," in *IEEE Nuclear Science Symposium and Medical Imaging Conference 2018 (IEEE NSS/MIC'18)*, Sydney, Australia, Nov. 2018.

[11] V. Grubsky, V. Romanov, E. Patton, and T. Jannson. (2012) Compton Imaging Tomography: A New Approch for 3D NDI of Complex Components. [Online]. Available: nasa.gov/sites/default/files/626746main_4A-3_Grubsky.pdf

[12] J. Callerame, "X-ray backscatter imaging: photography through barriers," *Powder diffraction*, vol. 21, no. 2, pp. 132–135, 2006.

[13] B. C. Towe and A. M. Jacobs, "X-ray backscatter imaging," *IEEE Transactions on Biomedical Engineering*, no. 9, pp. 646–654, 1981.

[14] P. G. Prado, M. K. Nguyen, L. Dumas, and S. X. Cohen, "Three-dimensional imaging of flat natural and cultural heritage objects by a Compton scattering modality," *Journal of Electronic Imaging*, vol. 26, no. 1, p. 011026, 2017, [doi:10.1117/1.JEI.26.1.011026].

[15] L. Lawson, "Compton X-ray backscatter depth profilometry for aircraft corrosion inspection," *Materials Evaluation*, vol. 53, no. 8, 8 1995.

[16] S. Naito, S. Yamamoto, and S. Yamamoto, "Novel X-ray backscatter technique for detecting crack below deposit," in *7th International Conference on NDE in Relation to Structural Integrity for Nuclear and Pressurized Components*, 2010.

[17] G. Rigaud, M. K. Nguyen, and A. K. Louis, "Circular harmonic decomposition approach for numerical inversion of circular Radon transforms," in *Proceedings of the 5th International ICST Conference on Performance Evaluation Methodologies and Tools*. ICST (Institute for Computer Sciences, Social-Informatics and Tools), 2011, pp. 582–591.

[18] ——, "Novel numerical inversions of two circular-arc Radon transforms in Compton scattering tomography," *Inverse Problems in Science and Engineering*, vol. 20, no. 6, pp. 809–839, 2012, [doi:10.1080/17415977.2011.653008].

[19] J. Cebeiro, M. K. Nguyen, M. Morvidone, and A. Noumowé, "New improved Compton scatter tomography modality for investigative imaging of one-sided large objects," *Inverse Problems in Science and Engineering*, vol. 25, no. 11, pp. 1676–1696, 2017, [doi:10.1080/17415977.2017.1281920].

[20] M. K. Nguyen and T. T. Truong, "Inversion of a new circular-arc Radon transform for Compton scattering tomography," *Inverse Problems*, vol. 26, no. 6, p. 065005, 2010, [doi:10.1088/0266-5611/26/9/099802].

[21] C. Tarpau and M. K. Nguyen, "Scattering imaging system with dual configurations," in *Fourteenth International Conference on Quality Control by Artificial Vision*, vol. 11172. International Society for Optics and Photonics, 2019, p. 111720Y.

[22] C. Tarpau, J. Cebeiro, M. Morvidone, and M. K. Nguyen, "A new concept of Compton Scattering tomography and the development of the corresponding circular Radon transform," *IEEE Transactions on Radiation and Plasma Medical Sciences*, vol. (accepted for publication), 2019, [10.1109/TRPMS.2019.2943555].

[23] T. CPrettyman, R. Gardner, J. Russ, and K. Verghese, "A combined transmission and scattering tomographic approach to composition and density imaging," *Applied radiation and isotopes*, vol. 44, no. 10-11, pp. 1327–1341, 1993.

[24] L.-T. Chang, "A method for attenuation correction in radionuclide computed tomography," *IEEE Transactions on Nuclear Science*, vol. 25, no. 1, pp. 638–643, 1978, [doi:10.1109/TNS.1978.4329385].

[25] A. Maze, R. Collorec, P. Bourguet, and M. Pierpittte, "Iterative reconstruction methods for non uniform attenuation distribution in SPECT," in *1992 14th Annual International Conference of the IEEE Engineering in Medicine and Biology Society*, vol. 5. IEEE, 1992, pp. 1821–1822, [doi:10.1109/IEMBS.1992.5762056].

[26] A. C. Kak and M. Slaney, *Principles of computerized tomographic imaging*. Society of Industrial and Applied Mathematics, 2001.

[27] G. Rigaud, R. Régnier, M. K. Nguyen, and H. Zaidi, "Combined modalities of Compton scattering tomography," *IEEE Transactions on Nuclear Science*, vol. 60, no. 3, pp. 1570–1577, 2013, [doi:10.1109/TNS.2013.2252022].

[28] O. A. O. Guerrero, G. Rigaud, R. Régnier, and M. K. Nguyen, "Attenuation correction in a new modality of Compton Scattering Tomography," in *Interdisciplinary Symposium on Signal and Systems for Medical Applications (ISSSMA)*, Paris, France, Jun. 2013.

[29] R. N. Bracewell, "Numerical transforms," *Science*, vol. 248, no. II May, pp. 697–704, 1990, [doi:10.1126/science.248.4956.697].